

Barriers on the EDGE: A scalable CBF architecture over EDGE for safe aerial-ground multi-agent coordination

Viswa Narayanan Sankaranarayanan*, Achilleas Santi Seisa, Akshit Saradagi,
Sumeet Satpute, and George Nikolakopoulos

Abstract—In this article, we address the problem of designing a scalable control architecture for a safe coordinated operation of a multi-agent system with aerial (UAVs) and ground robots (UGVs) in a confined task space. The proposed method uses Control Barrier Functions (CBFs) to impose constraints associated with (i) collision avoidance between agents, (ii) landing of UAVs on mobile UGVs, and (iii) task space restriction. Further, to account for the rapid increase in the number of constraints for a single agent with the increasing number of agents, the proposed architecture uses a centralized-decentralized Edge cluster, where a centralized node (Watcher) activates the relevant constraints reducing the need for high onboard processing and network complexity. The distributed nodes run the controller locally to overcome latency and network issues. The proposed Edge architecture is experimentally validated using multiple aerial and ground robots in a confined environment performing a coordinated operation.

I. INTRODUCTION

Deployment of a coordinated multi-robot system comprising of multiple ground and aerial agents requires imposition of various safety constraints, both within the ground and aerial layers and between the ground and aerial layers. In a multi-agent scenario with heterogeneous agent mobilities, three challenges are typically faced: (a) reliable imposition of safety, (b) establishing environmental awareness for each agent, and (c) scaling the control architecture for large number of agents [1], [2]. In the past decade, design of safe and scalable multi-agent control architectures has generated keen interest, especially in the robotics community, where many multi-agent applications are safety-critical. In this work, we consider a multi-agent system with both UAV and UGV agents, where imposing several state constraints is crucial, specifically to avoid collisions with other agents, force UAVs to land safely on UGVs, while remaining inside a confined pre-specified task space.

In recent years, Control Barrier Function (CBF) approach has emerged as a popular choice for imposing safety constraints over dynamical systems [3][4]. The CBF approach derives safe control inputs that render a set of safe robot configurations forward invariant, by filtering a nominal goal-reaching controller. In the context of this article, the constraints arise as i) safety constraints associated with collision avoidance in the aerial and ground layers, ii) constraints

associated with safe landing of aerial robots on ground robots, and iii) constraints restricting operation within a pre-specified task space. The constraints associated with every robot (ground and aerial) are transformed into safe sets and the corresponding control barrier functions are formulated. Then, for every agent, a time-varying set of CBFs are simultaneously imposed by a CBF filter, in order to render the intersections of the safe sets forward invariant. The CBF filtered control signal is minimally invasive on the nominal controller and is derived by solving a computationally-light quadratic optimization problem (QP) defined over the space of control inputs.

While popular CBF techniques for multi-agent systems involve a centralized controller [5], [6], [7], the main disadvantage of the design is that a major part of the control layer runs offboard, jeopardizing the robot's nominal operation due to networking issues. Although centralized control excels in performance, its scalability limitations make it impractical for large-scale multi-agent systems [8], [9]. In contrast, the distributed control problem [10], [11] improves the onboard safety of the robots but demands the robots to possess the knowledge of other agents and the environment.

Practically, gathering the knowledge of other agents and the environment involves communication overheads, network complexity and heavy onboard processing. For every additional agent, the communication links, constraints, and computational demand increases rapidly [12]. Moreover, the communication links and constraints must be dynamically updated on every single agent, when a new agent is added or removed in the system. Further, computational demand can be reduced by using only the relevant constraints, which potentially impact an agent. Therefore, the system needs a mixed architecture, which captures the advantages of both strategies. On this line, the Model Predictive Control implementation in [13] exploits a hybrid distributed and centralized approach to harness the advantages of both strategies. Inspired by this notion, there is a need for a hybrid control implementation for multi-agent systems that improves the computational capability and the scalability of the solution. In this line, Edge computing that enables high computing with low latency has evolved to be a practical method to offload a part of processing [14].

Contributions: Given this premise, we present the following major contributions in this work: (a) Design of a CBF-based controller for each agent for enforcing collision avoidance and safe landing of UAVs on their respective UGVs using a novel time-varying landing CBF. (b) A centralized-

*Corresponding author

The authors are with the Robotics and Artificial Intelligence Group of the Department of Computer Science, Electrical and Space Engineering at Luleå University of Technology, Sweden. This work has been partially funded by the European Unions Horizon 2020 Research and Innovation Programme AERO-TRAIN under the Grant Agreement No. 953454.

distributed Edge architecture featuring all the individual controller nodes as distributed clients, and a centralized server node, which accumulates all the information to decide the constraints and communicate the same with each of the clients. (c) An experimental validation of the proposed architecture using multiple UAVs and UGVs.

II. PROBLEM FORMULATION

In this section, the aerial (UAV) and ground (UGV) robots are modeled, the constraints necessary to enable safe coordination are identified, and the overall control problem is formulated.

A. Modeling of the UAV

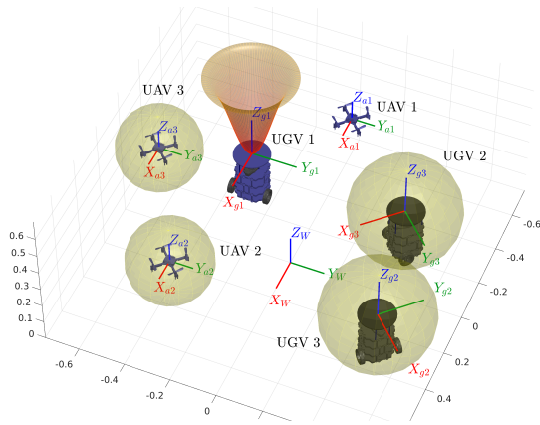


Fig. 1: A schematic of robots with their associated coordinate frames and UAV 1's safety constraints.

The dynamics of a UAV with its body frame $\mathbf{X}_{ai} - \mathbf{Y}_{ai} - \mathbf{Z}_{ai}$ is given by,

$$m_i \ddot{\mathbf{p}}_{ai}(t) + m_i \mathbf{G} = \mathbf{f}_i, \quad (1a)$$

$$J_i(q_i(t)) \ddot{q}_i(t) + C_i(q_i, \dot{q}_i, t) \dot{q}_i(t) = \boldsymbol{\tau}_i, \quad (1b)$$

where $\mathbf{p}_{ai}(t) \triangleq [x_{ai}(t), y_{ai}(t), z_{ai}(t)]^T \in \mathbb{R}^3$, $q_i(t) \triangleq [\phi_i(t), \vartheta_i(t), \psi_i(t)]^T$ represents the position and orientation of the UAV in the inertial frame $(\mathbf{X}_W - \mathbf{Y}_W - \mathbf{Z}_W)$; $\mathbf{G} \triangleq [0, 0, -g]^T \in \mathbb{R}^3$ is the gravity vector; $\mathbf{f}_i \in \mathbb{R}^3$ is the position control inputs in the inertial frame, (cf. Fig. 1); m_i is the mass and $J_i, C_i \in \mathbb{R}^{3 \times 3}$ are the inertia and Coriolis matrices; $\boldsymbol{\tau}_i \in \mathbb{R}^3$ is the attitude control input of the i^{th} UAV for $i \in \{1, \dots, N\}$ and N is the total number of UAVs.

B. Modeling the Ground Robot

Since UGVs in general are non-holonomic, we consider a differential-drive unicycle model for the UGVs as given below.

$$\begin{bmatrix} \dot{x}_{gi} \\ \dot{y}_{gi} \\ \dot{\theta}_i \end{bmatrix} = \begin{bmatrix} \cos(\theta_i) & 0 \\ \sin(\theta_i) & 0 \\ 0 & 1 \end{bmatrix} \begin{bmatrix} v_i \\ \omega_i \end{bmatrix}, \quad \begin{bmatrix} v_i \\ \omega_i \end{bmatrix} = \begin{bmatrix} \frac{R_{1i} + R_{2i}}{2} \\ \frac{R_{1i} - R_{2i}}{2L} \end{bmatrix} \quad (2)$$

where $[x_{gi} \ y_{gi}]^T$ form the position vector, θ_i represents the heading of the UGV in the inertial frame, v_i, ω_i represent the linear and angular velocities in the body frame, and

R_{1i}, R_{2i} represent the velocities of the right and left wheels respectively of the i^{th} UGV and L is the distance between the two wheels of the UGV. The body frame is represented by $\mathbf{X}_{gi} - \mathbf{Y}_{gi} - \mathbf{Z}_{gi}$.

C. Constraint Identification

In this article, we consider the scenario where there are N UAV-UGV pairs that perform their predefined tasks. When a landing signal is provided, the UAVs return to their corresponding UGVs and land on them while the UGVs continue to perform their tasks. Therefore, the constraints can be broadly classified into interactions in the aerial layer (AA) between the UAVs, the interactions between the ground layer (GG) between the UGVs, and the aerial-ground interactions (AG) between the UAVs and the UGVs. The latter is further classified into the interaction of a UAV with its corresponding UGV (AGC) and the interactions of the UAV with other UGVs (AGO). It is intuitive that AA, GG and AGO are merely collision avoidance constraints between different agents for safely performing their high-level tasks. The AA constraints for the UAV-pair (i, j) is represented with their relative displacements r_{aij} as,

$$r_{aij}^2 \geq s_a^2, \quad r_{aij} = p_{ai} - p_{aj} \quad (3)$$

where $s_a > 0$ is the desired safety radius between two UAVs. Similarly, for AGO constraint, the relative displacement r_{ij} between i^{th} UAV and j^{th} UGV must be outside a safety radius, $s_{ag} > 0$ given by,

$$r_{ij}^2 \geq s_{ag}^2, \quad r_{ij} = p_{ai} - p_{gj}. \quad (4)$$

Since ground robots are restricted to two dimensions, GG constraint becomes a circle in the XY -plane given by,

$$r_{gij}^2 \geq s_g^2, \quad r_{gij} = \rho_{gi} - \rho_{gj}, \quad (5)$$

where $s_g > 0$ is the safety radius, and $\rho_{gi} = [x_{gi} \ y_{gi}]^T$ is the horizontal position of the UGV. Unlike these constraints, AGC cannot be simplified into a collision avoidance problem because while the constraint must restrict the i^{th} UAV from colliding with the i^{th} UGV, it must still allow the UAV to approach the UGV vertically and establish a contact. Hence, we extend our descending constraint from [15] to a moving target scenario, which demands a time-varying constraint.

$$r_{zi}(t) \geq \beta \alpha l_i(t) \exp(-\alpha l_i(t)) + \gamma, \quad (6)$$

where $(r_{xi}, r_{yi}, r_{zi})^T \triangleq p_{ai} - p_{gi} \in \mathbb{R}^3$ define the relative displacement between the i^{th} UAV-UGV pair, $l_i = r_{xi}^2(t) + r_{yi}^2(t)$ is their corresponding squared horizontal distance, α, β are scaling factors in the horizontal and vertical directions respectively and γ is an offset to avoid the turbulence from the landing platform. In this setup, Eq. (4) distances other UAVs from the i^{th} UGV clearing out the space around the i^{th} UGV for a conflict-free landing. Additionally, we apply box constraints on all the agents to replicate an indoor environment with walls and roof as given below,

$$\underline{x} < x_{ai} < \bar{x}, \quad \underline{y} < y_{ai} < \bar{y}, \quad \underline{z} < z_{ai} < \bar{z}, \quad (7a)$$

$$\underline{x} < x_{gi} < \bar{x}, \quad \underline{y} < y_{gi} < \bar{y}, \quad (7b)$$

where $x, \bar{x}, y, \bar{y}, z, \bar{z}$ form the maximum and minimum bounds for the states. Further, we highlight the necessary assumptions for formulating the control problem.

Assumption 1 (Minimum distance between UGVs): The safety radii magnitudes must be such that, $s_g > s_{ag} > s_a$.

Assumption 2 (Velocity of UGVs): The linear and angular velocities of the UGVs are smooth and bounded, such that $|v_i| < \bar{v}, |\omega_i| < \bar{\omega}$. Further, the UGVs move on a flat surface that $\dot{z}_{gi} = 0 \forall i \in \{1, 2, \dots, N\}$.

Remark 1: Assumption 1 is standard since the landing platforms are sufficiently larger than the cross-sectional area of the UAVs. In its absence, the AA and AGO constraints will restrain the UAVs from landing on the UGVs. Further, the upper bound on the velocities in Assumption 2 translates to $|\dot{x}_{gi}|, |\dot{y}_{gi}| < \bar{v}$, which is essential for the UAV to track and land on its UGV.

While latency and momentary loss of communication make an offboard control scheme unreliable, the onboard controllers are limited by computing power. Since the number of constraints per UAV is $2N + 4$ for N UAV-UGV pairs ($N + 3$ for UGVs), it is optimal to consider only the proximal interactions (say within 1 m) for AA, GG and AGO. However, deciding the number of constraints also requires the knowledge of every agent, which increases the computational load and number of connections between the agents. Moreover, the interaction constraints AA, GG, AGO and AGC in (3) - (6) are nonconvex in nature. Given these challenges, let us formulate the control problem.

Problem Formulation: Design a control architecture for the coordinated operation of multi UAV-UGV pairs defined by the dynamics in Eq. (1) - (2) and safe landing of UAVs on their respective mobile UGVs enforcing the constraints in Eq. (3) - (7) under the assumptions 1 & 2.

III. EDGE-ENABLED CONTROL ARCHITECTURE

Having discussed the control challenge, we formally introduce the proposed control architecture, which suitably accommodates the constraints and minimizes the onboard computations and number of connections between the agents.

A. Edge Architecture

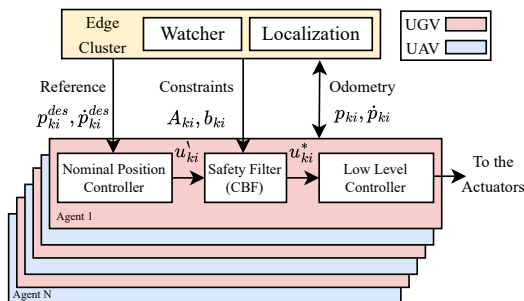


Fig. 2: Edge architecture. Each robot has its own distributed control unit, and receives CBF constraints and its position estimation from the edge cluster.

In the considered scenario, Edge computing provides the benefit of distributed onboard control and a centralized decision processing unit [16]. Here, the UAVs and UGVs function as edge devices (clients) of the system, while the edge cluster (server) provides the computational capacity [14]. The control architecture consists of three main segments: the CBF-enabled control unit, the data acquisition and localization unit, and a remote monitoring and decision-making unit (referred as Watcher). The control units are distributed to run onboard on the edge clients. Since computational power is a trade-off on the onboard computers, we use first-order CBFs to impose the safety constraints. The design of the control unit is further discussed in Subsection III-B.

We deploy N UAV-UGV pairs ($2N$ agents) and establish an edge cluster to offload the localization method of all agents, along with the Watcher, as depicted in Fig. 2. We enable communication between the agents through Wi-Fi connectivity. The localization unit either uses an external positioning system (as in our experimental setup) or performs a global SLAM using the agents' onboard sensor information to estimate the pose of each agent. The Watcher node accesses the localization unit and identifies the proximal agents to each of the robots and generates its constraint matrix. As such, each agent's control unit requires only its global localization and setpoints for the nominal controller, and the constraint matrices to enforce safety. Since no further information is required for safe interaction among agents, the proposed topology supports a simplified connectivity structure, thereby facilitating streamlined communication, enabling scalability, and reducing throughput.

The scalability of the proposed architecture is driven by two main factors, thanks to the hybrid nature of edge computing. (a) Number of communication links: The proposed star topology requires links equal to the number of agents, i.e., $2N$ (UAV and UGV), since agents exchange information only with the Watcher. In contrast, fully distributed systems demand fully connected topologies, making the number of links equal to $2N \times (2N - 1)$. (b) Computational capacity: Distributed computational processing allows for effective management of computational resources depending on the number of proximal agents.

B. Distributed Control Units

This section presents the distributed control unit for UAVs and UGVs. The control unit is divided into three layers: a nominal position controller, a CBF-based safety filter, and a low-level controller. The position controller produces nominal velocity inputs to reach the setpoints ($p_{ai}^{des} \in \mathbb{R}^3, p_{gi}^{des} \in \mathbb{R}^2$) given by, $u_{ai}' = -K_{ai}(p_{ai} - p_{ai}^{des}) + \dot{p}_{ai}^{des}$, $u_{gi}' = -K_{gi}(p_{gi} - p_{gi}^{des}) + \dot{p}_{gi}^{des}$, where K_{ai}, K_{gi} are positive definite gain matrices. This input is filtered using first-order CBF constraints to obtain the filtered velocity input $u_{ai}^* \in \mathbb{R}^3, u_{gi}^* \in \mathbb{R}^2$ as will be explained in Section IV. The UAV's filtered velocity inputs are tracked by a low-level controller (cf. [15] Section III).

Since the CBF filter uses first-order constraints, it uses the first-order kinematics of the robots during optimization. The UAV's first-order kinematics simplifies to $\dot{p}_{ai} = u_{ai}(t)$.

However, since UGV is non-holonomic, we use the Near-identity diffeomorphism (NID) presented in [17], [18] to get its single integrator approximation given by,

$$\begin{bmatrix} x_{oi} \\ y_{oi} \end{bmatrix} = \begin{bmatrix} x_{gi} \\ y_{gi} \end{bmatrix} + o_i \begin{bmatrix} \cos(\theta_i) \\ \sin(\theta_i) \end{bmatrix}, \quad (8)$$

$$\implies \begin{bmatrix} v_i \\ \omega_i \end{bmatrix} = \begin{bmatrix} \cos(\theta_i) & \sin(\theta_i) \\ -\frac{\sin(\theta_i)}{o_i} & \frac{\cos(\theta_i)}{o_i} \end{bmatrix} \begin{bmatrix} \dot{x}_{oi} \\ \dot{y}_{oi} \end{bmatrix} \quad (9)$$

where $o_i > 0 \in \mathbb{R}^+$. Geometrically, $\rho_{oi} = [x_{oi} \ y_{oi}]^\top$ represents a 2D point (offset) at a distance of o_i from the i^{th} UGV's origin along the \mathbf{X}_{gi} axis. By choosing a sufficiently small o_i , the same constraints could be used in the offset space. It is to be remarked that converting the dynamics using NID retains the same nominal control input, which is passed on to the CBF layer. The filtered velocity input $u_{gi}^* \in \mathbb{R}^2$ obtained from the CBF layer is reconverted to the UGV's body frame using Eq. (9), which is used for actuating the wheel motors based on the relationship in (2).

IV. CBF IMPLEMENTATION

Now that the overall control architecture is described, this section presents the CBF filter implementation inside a distributed control node and its constraint matrices. As discussed in the earlier sections, though the safety constraints are imposed by the distributed control node through quadratic programming, the constraint matrices for every distributed control unit are updated by the Watcher node using ROS messages. Since every distributed control unit handles the control inputs of only the specific robot, the constraints that use the position of other agents become time-varying. So, let us formally define the time-varying control barrier function before formulating the CBFs, and subsequently forming the quadratic program.

Let the time-varying safe set for a given affine dynamical system, $\dot{x}(t) = f(x(t)) + g(x(t))u(t)$ be defined by the state space region, $\mathcal{S}(t) \subset \mathcal{X}$, where $x \in \mathcal{X} \subset \mathbb{R}^n, u \in \mathbb{U} \subset \mathbb{R}^m, f, g$ are Lipschitz continuous. Now, a continuously differentiable function $h(x, t) : \mathcal{D}(t) \subset \mathcal{X} \rightarrow \mathbb{R}$, such that $\mathcal{S}(t) = \{x \in \mathcal{X} | h(x, t) \geq 0\}$ ($\mathcal{S}(t)$ is a zero-level super set of $h(x, t) \forall t$), renders the set $\mathcal{S}(t)$ safe if the control input u ensures positive invariance of the set $\mathcal{S}(t) \forall t$, i.e., $x(t_0) \in \mathcal{S}(t_0)$ implies $x(t) \in \mathcal{S}(t) \forall t \geq t_0$. Moreover, if the safe set, $\mathcal{S}(t)$ is rendered asymptotically stable when $x(t)$ is initialized outside the unsafe set ($x(0) \in \mathcal{D}(0) \setminus \mathcal{S}(0)$), a measure of robustness can be incorporated into the notion of safety. The condition validating the continuous function, $h(x, t)$ as a control barrier function, is presented in the following definition.

Definition 1 (Time-varying CBF): A candidate function $h(x, t)$ is a valid control barrier function for an affine dynamical system, $\dot{x} = f(x, t) + g(x, t)u$ if there exists a locally Lipschitz continuous class- \mathcal{K}_∞ function ξ , such that $\forall(x, t) \in \mathcal{D}(t) \times [0, \infty]$

$$\sup_{u \in \mathcal{U}} \frac{\partial h(x, t)}{\partial x} (f(x) + g(x)u) + \frac{\partial h(x, t)}{\partial t} \geq -\xi(h(x, t)) \quad (10)$$

Remark 2: The condition in (10) captures the forward invariance of $\mathcal{S}(t)$ ($\dot{h}(x, t) \geq 0$ on $\partial \mathcal{B}(t)$), and the asymptotic stability of $\mathcal{S}(t)$ ($\dot{h}(x, t) \geq 0$ in $\mathcal{D}(t) \setminus \mathcal{S}(t)$).

Now, the CBF design for the safety constraints are discussed in Subsections IV-A - IV-C. Subsequently, the quadratic programming is formed with appropriate constraints in Subsection IV-D.

A. Spherical CBF

The inequalities in (3) - (4) form spherical and (5) form circular constraints for the robots. Therefore, we derive the following candidate functions.

$$h_{aij} = r_{aij}^2 - s_a^2, \quad h_{gij} = r_{oij}^2 - s_g^2, \quad h_{agij} = r_{ij}^2 - s_{ag}^2, \quad (11)$$

where $r_{oij} = (\rho_{oi} - \rho_{oj})$ is the relative distance between the offsetted positions of the UGVs. It is to be remarked that since these constraints depend on the time-varying positions of other robots, which are external to the particular robot's system, the CBFs are time-varying. Through Definition 1, it can be shown that the candidate CBFs (11) are valid time-varying CBFs for the UAV's and UGV's respective admissible control sets of $\mathcal{U}_a = [-\bar{v}, \bar{v}] \times [-\bar{v}, \bar{v}] \times [-\bar{v}, \bar{v}]$ and $\mathcal{U}_g = [-v_g, v_g] \times [-v_g, v_g]$, where $0 < v_g < \bar{v}$. Provided the UAVs and UGVs initiate with a distance between them larger than their respective safety radii, they do not get closer than their respective safety radii throughout the time, thus avoiding possible collisions, due to the virtue of forward invariance of the CBFs.

B. Landing CBF

For the AGC constraint, a candidate function is formed as,

$$h_{lii} = r_{zi} - \beta \alpha l_i \exp(-\alpha l_i) - \gamma \quad (12)$$

Unlike [15], h_{lii} is time-varying as it depends on an UGV's time-varying position. Further, their gradients are given by,

$$\frac{\partial h_{lii}}{\partial p_{ai}} = [k r_{xi} \quad k r_{yi} \quad 1]^\top, \quad \frac{\partial h_{lii}}{\partial t} = -k(r_{xi}\dot{x}_{gi} + r_{yi}\dot{y}_{gi}) \quad (13)$$

where $k = 2\beta\alpha(\alpha l_i - 1)\exp(-\alpha l_i)$. Therefore, the candidate function in (12) can be proven to be a valid time-varying CBF using Definition 1 for the UAV's admissible control set of $\mathcal{U}_a = [-\bar{v}, \bar{v}] \times [-\bar{v}, \bar{v}] \times [-\bar{v}, \bar{v}]$. Since the CBF possesses the forward invariance property, when the UAVs are initiated in the safe region defined by the zero super level set $\mathcal{S}_i = \{p_{ai} \in \mathbb{R}^3 | h_{lii,t} \geq 0\}$, they remain in the safe region during the landing process, which forces them to vertically descend through a funnel-like region above the landing platform.

C. Box CBF

The box inequalities in (7) form the following functions.

$$b_{a1i} = \bar{x} - x_{ai}, \quad b_{a2i} = x_{ai} - \underline{x}, \quad b_{a3i} = \bar{y} - y_{ai}, \quad (14a)$$

$$b_{a4i} = y_{ai} - \underline{y}, \quad b_{a5i} = \bar{z} - z_{ai}, \quad b_{g1i} = \bar{x} - x_{oi}, \quad (14b)$$

$$b_{g2i} = x_{oi} - \underline{x}, \quad b_{g3i} = \bar{y} - y_{oi}, \quad b_{g4i} = y_{oi} - \underline{y}. \quad (14c)$$

A separate CBF for the lower bound of the UAV's altitude is redundant as the AGC constraint in (12) maintains the UAV above the landing platform [15]. Unlike other constraints, the

box constraints are time-invariant. Using similar arguments in the previous subsections, the functions in (14) are proven to be valid control barrier functions. So, the UAVs and UGVs remain inside the box if they are initiated within it.

D. CBF Safety Filter for i^{th} Agent

The safety filter running on the distributed control units takes in the nominal input $u'_{ki}(p_{ki}(t), t) \forall k \in \{d, g\}$, and generates a filtered input u^*_{ki} , which satisfies the safety constraints. This action is performed by a quadratic program:

$$\begin{aligned} u^*_{ki}(p_{ki}(t), t) = \operatorname{argmin}_{u_{ki} \in \mathcal{U}_k} & \|u_{ki} - u'_{ki}(p_{ki}(t), t)\| \\ \text{s.t.} : & \mathbf{A}_{ki} u_{ki} \geq -\mathbf{b}_{ki}. \end{aligned} \quad (15)$$

The constraint in (15) is derived using (10) and the first-order approximations of the robots where $f(x) = 0, g(x) = \mathbf{I}, \mathbf{A} = \frac{\partial h}{\partial x}, \mathbf{b} = \xi(h, t) + \frac{\partial h}{\partial t}$. As mentioned in the control architecture, the matrices $\mathbf{A}_{ki}, \mathbf{b}_{ki} \forall k \in \{a, g\}$ are generated for each control unit by the Watcher node using the following algorithm. $\mathbf{A}_{ki}, \mathbf{b}_{ki}$ are initialized with zeros of size $(C \times 3), (C)$ respectively. Then the boundary constraints are updated to $\mathbf{A}_{ki}, \mathbf{b}_{ki}$, followed by AG or GG constraints. If it is an UAV, AGC and AA constraints are added.

Algorithm 1 Constraint Matrix Update Algorithm

- 1: **Input:** i, k, C ; **Output:** $\mathbf{A}_{ki}, \mathbf{b}_{ki}$
 - 2: $[\mathbf{A}_{ki}, \mathbf{b}_{ki}] \leftarrow [0] * (C \times 4)$
 - 3: **for** $j \leftarrow 1$ to C **do**
 - 4: $[\mathbf{A}_{ki}[j], \mathbf{b}_{ki}[j]] \leftarrow \left[\left[\frac{\partial b_{kji}}{\partial p_{ki}} \right]^T, \xi(b_{kji}) + \frac{\partial b_{kji}}{\partial t} \right]$
 - 5: **end for**
 - 6: **for** $n \leftarrow 1$ to N **do**
 - 7: **if** i is not n and $\|p_{ki} - p_{gn}\| < 1$ **then**
 - 8: Append $\left[\left[\frac{\partial h_{kgin}}{\partial p_{ki}} \right]^T, \xi(h_{kgin}) + \frac{\partial h_{kgin}}{\partial t} \right]$ to $[\mathbf{A}_{ki}, \mathbf{b}_{ki}]$
 - 9: **end if**
 - 10: **end for**
 - 11: **if** k is d **then**
 - 12: Append $\left[\left[\frac{\partial h_{iij}}{\partial p_{ki}} \right]^T, \xi(h_{iij}) + \frac{\partial h_{iij}}{\partial t} \right]$ to $[\mathbf{A}_{ki}, \mathbf{b}_{ki}]$
 - 13: **for** $n \leftarrow 1$ to N **do**
 - 14: **if** i is not n and $\|p_{ki} - p_{an}\| < 1$ **then**
 - 15: Append $\left[\left[\frac{\partial h_{ain}}{\partial p_{ki}} \right]^T, \xi(h_{ain}) + \frac{\partial h_{ain}}{\partial t} \right]$ to $[\mathbf{A}_{ki}, \mathbf{b}_{ki}]$
 - 16: **end if**
 - 17: **end for**
 - 18: **end if**
-

The partial derivatives of the CBFs in (11) & (14) are not explicitly mentioned, because they are trivial.

V. EXPERIMENTAL VALIDATION

A. Experiment Design

An experimental setup involving three UGVs (Turtlebot3 Burger) and three UAVs (Crazyflie 2) is designed to validate the control architecture. The agents operate in a confined region of dimension $2.8 \text{ m} \times 2.8 \text{ m} \times 2 \text{ m}$. The UGV's control units run in their on-board computers that have a

Quad Core 1.2GHz - 64bit CPU and 1GB RAM each. The UAV's clients run inside docker containers with CPU and memory limitations. The ROS-based edge cluster runs on an external computer and the localization is provided by a motion capture system.

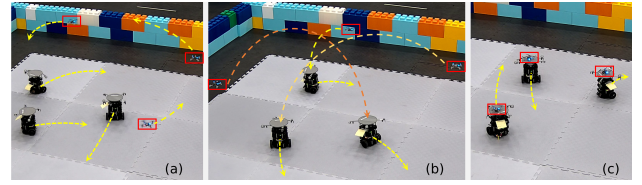


Fig. 3: Red boxes showing the UAVs, and arrows pointing at robots' directions of motion: (a) Robots follow their path. (b) UAVs initiate to land. (c) UAVs land successfully.

The UAVs initially move along a circular path around the center at an altitude of 0.35 m above the UGVs (cf. Fig. 3). Meanwhile, the UGVs move along their pre-defined trajectories $\rho_{g1} = [0.3 \sin(0.1t), \cos(0.1t)]^T$, $\rho_{g2} = [\cos(0.1t), \sin(0.1t)]^T$, $\rho_{g3} = [-\cos(0.1t), -0.3 \sin(0.1t)]^T$. When the landing signal is given, the UAVs approach their corresponding UGVs. In this experiment the following control parameters are used: $s_a = 0.4 \text{ m}$, $s_g = 0.8 \text{ m}$ and $s_{ag} = 0.6 \text{ m}$, $\alpha = 12$, $\beta = 1.2$, $\gamma = 0.06 \text{ m}$, $\bar{x} = \bar{y} = 1.3 \text{ m}$, $\bar{z} = 2 \text{ m}$, $\underline{x} = \underline{y} = -1.3 \text{ m}$, $o_i = 0.1 \text{ m} \forall i \in \{1, 2, 3\}$, the proximal distance to include a constraint is chosen to be 1m. The motors are slowed down to complete the landing when $\|(r_{xii}, r_{yii})^T\| < 0.01 \text{ m} \ \& \ r_{zii} < 0.07 \text{ m}$.

B. Experimental Results

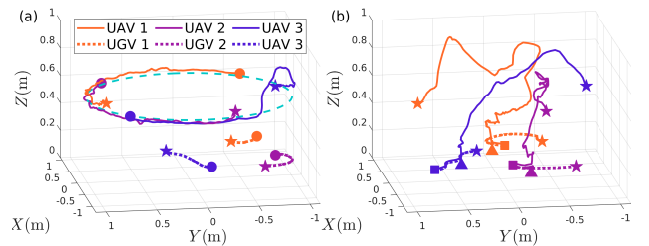


Fig. 4: Paths traced by the UAVs and UGVs: (a) before the signal to land, (b) after the landing signal. Circular markers represent the initial positions, stars show the positions at which landing signal is given, triangles are the positions where UAVs land, and squares are the ends of paths. Cyan circle in (a) is the UAV's desired path.

Figure 4 shows the robots' paths in the inertial frame. Fig. 5 highlights the relative motions between the agents. The shapes in the center represent the CBF boundaries, fixed to one of the two robots constrained by the CBFs. The instantaneous values of CBFs are presented in Fig. 6. Due to space limitations, the evolution of CBFs are presented only for a representative sample. It is noticeable in Fig. 4 (a) that when the UAV 3 flies over UGV 2, the AGO CBF h_{ag32} approaches zero (Fig. 6 (e) at 8 s), so the controller increases the UAV's altitude, which is also reflected in Fig.

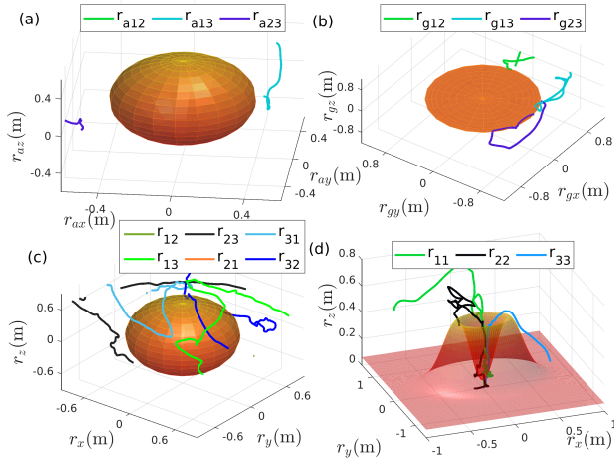


Fig. 5: Performance of the CBFs: (a), (b), (c) & (d) present AA, GG, AGO & AGC constraints respectively.

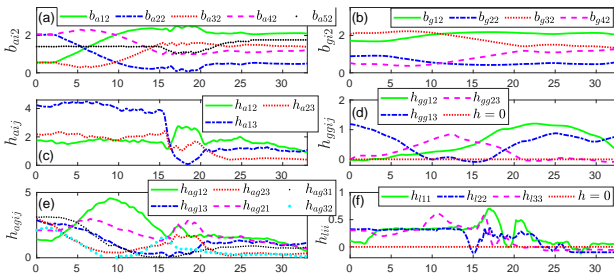


Fig. 6: Evolution of the CBFs over time (seconds).

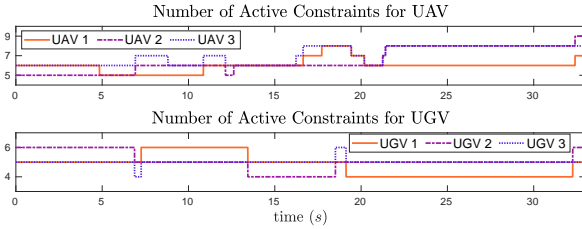


Fig. 7: Number of active constraints for each robot.

5 (c), where (r_{32}) shows the motion UAV 3 relative to UGV 2's position. Other UAVs follow the desired paths because there is no conflict in their path.

When the landing signal is given (around 15 s), UAV 1 increases its altitude to fly over UGV 3 due to AGO as seen in Fig. 4 (b). The same is observed from the green line (r_{13}) in Fig. 5 (c). When UAV 1 nears UGV 1, the controller increases its altitude to enter the funnel. UAV 2 temporarily enters the unsafe zone when landing is initiated ($h_{122} < 0$ in Fig. 6 (j) at 15 s). So, it is pushed outside rapidly by the controller to make $h_{122} > 0$. The AGC CBF smoothly guides it to vertically align with its UGV and descend. A similar trend is observed when UAV 3 flies over UGV 1 in Fig. 5 (c) light blue line (r_{31}) . In Fig. 6 (f), it is noticed that all AGC CBFs approach zero and immediately increase when the UAVs approach the CBF boundary, where they increase their altitude to enter the funnel from the top. When the UAVs approach the funnel's tip, h_{1ii} in Fig. 6 (f) oscillates near zero due to the mechanical limitations of the UAVs and

settles slightly below zero when the landing is completed.

Though the NID approximation for the UGVs work decently, the UGV's actual position enters the unsafe region momentarily (Fig. 5 (b), (h_{g13}, h_{g23}) in Fig. 6 (d)). However, considering this effect, an additional margin is included in the safety radius s_g to ensure UGVs' safety. Since other relative distances are larger than the figure margins, they do not appear in Fig. 5 (a) - (c). The box CBFs in Fig. 6 (a) - (b) remain positive, proving that the robots maintained their boundary conditions even while handling conflicts. It is to be remarked that in Fig. 6, though the values are plotted for all time instances, the AA, GG and AGC CBFs are deactivated when their corresponding relative distances are more than 1 m. The number of active constraints along time is plotted in Fig. 7 for additional information.

C. Discussions on conflicts and scalability

Even though a small number of robots were used in the experimental validation within a confined region, the number of active constraints changes with time for every robot (cf. Fig. 7). Further, the instances where a UAV is in close-proximity to more than 4 other robots are minimal. In such a scenario, opting to consider all constraints as active, or accumulating all the localization information on every distributed node to determine the set of active constraints increases the computational demand without any significant improvements in the performance. In the multi-agent architecture proposed in this article, the Watcher node in the Edge cluster updates the constraints for each agent depending on the proximity of the agents and communicates the set of active constraints. Since the CBF filter runs on each of the robots, momentary communication delays or dropped packages from the server do not affect the overall performance of the control architecture. Since the only communication between the agents and the Watcher node are their odometry, reference, and constraint updates, adding or removing N agents only adds or removes N communication links and $3N$ ROS connections in the overall network. Further, the existing robots need not update their onboard controllers. Only the Localization and Watcher nodes must update themselves. Even in the confined operating region, the number of constraints for individual control units remains small for the majority of the time.

VI. CONCLUSION

In this work, we have addressed the problem of safe multiple UAV-UGV coordinated operation, and landing. We have identified the necessary constraints for enforcing safety and formulated the CBFs. To reduce the computational load in the onboard controller, we have designed an Edge architecture, where a centralized Localization node accumulates the odometry of all the robots, a Watcher node frames the constraint matrices, and distributed nodes run the safety-enhanced controller onboard locally using a quadratic program with the received constraints to produce minimally invasive control inputs. The proposed architecture is experimentally validated using multiple pairs of UAVs and UGVs. The results are analyzed thoroughly.

REFERENCES

- [1] M. Georgeff, "Communication and interaction in multi-agent planning," in *Readings in distributed artificial intelligence*. Elsevier, 1988, pp. 200–204.
- [2] Z. Song, Z. Wu, and H. Huang, "Safety-critical containment control for multi-agent systems with communication delays," *IEEE Transactions on Network Science and Engineering*, 2024.
- [3] A. D. Ames, S. Coogan, M. Egerstedt, G. Notomista, K. Sreenath, and P. Tabuada, "Control barrier functions: Theory and applications," in *2019 18th European Control Conference (ECC)*, 2019, pp. 3420–3431.
- [4] K. Garg, J. Usevitch, J. Breeden, M. Black, D. Agrawal, H. Parwana, and D. Panagou, "Advances in the theory of control barrier functions: Addressing practical challenges in safe control synthesis for autonomous and robotic systems," *Annual Reviews in Control*, vol. 57, p. 100945, 2024. [Online]. Available: <https://www.sciencedirect.com/science/article/pii/S1367578824000142>
- [5] R. Cheng, M. J. Khojasteh, A. D. Ames, and J. W. Burdick, "Safe multi-agent interaction through robust control barrier functions with learned uncertainties," in *2020 59th IEEE Conference on Decision and Control (CDC)*. IEEE, 2020, pp. 777–783.
- [6] L. Lindemann and D. V. Dimarogonas, "Control barrier functions for multi-agent systems under conflicting local signal temporal logic tasks," *IEEE control systems letters*, vol. 3, no. 3, pp. 757–762, 2019.
- [7] Y. Chen, A. Singletary, and A. D. Ames, "Guaranteed obstacle avoidance for multi-robot operations with limited actuation: A control barrier function approach," *IEEE Control Systems Letters*, vol. 5, no. 1, pp. 127–132, 2020.
- [8] J. Hu, A. Bruno, D. Zegieboylo, M. Zhao, B. Ritchken, B. Jackson, J. Y. Chae, F. Mertl, M. Espinosa, and C. Delimitrou, "To centralize or not to centralize: A tale of swarm coordination," *arXiv preprint arXiv:1805.01786*, 2018.
- [9] F. Bertilsson, M. Gordon, J. Hansson, D. Möller, D. Söderberg, Z. Zhang, and K. Åkesson, "Centralized versus distributed nonlinear model predictive control for online robot fleet trajectory planning," in *2022 IEEE 18th International Conference on Automation Science and Engineering (CASE)*. IEEE, 2022, pp. 701–706.
- [10] X. Tan and D. V. Dimarogonas, "Distributed implementation of control barrier functions for multi-agent systems," *IEEE Control Systems Letters*, vol. 6, pp. 1879–1884, 2021.
- [11] S. Zhang, K. Garg, and C. Fan, "Neural graph control barrier functions guided distributed collision-avoidance multi-agent control," in *Conference on robot learning*. PMLR, 2023, pp. 2373–2392.
- [12] A. S. Seisa, B. Lindqvist, S. G. Satpute, and G. Nikolakopoulos, "E-cnmpc: Edge-based centralized nonlinear model predictive control for multiagent robotic systems," *IEEE Access*, vol. 10, pp. 121 590–121 601, 2022.
- [13] J. Zhan, Z. Ma, and L. Zhang, "Data-driven modeling and distributed predictive control of mixed vehicle platoons," *IEEE Transactions on Intelligent Vehicles*, 2022.
- [14] A. S. Seisa, G. Damigos, S. G. Satpute, A. Koval, and G. Nikolakopoulos, "Edge computing architectures for enabling the realisation of the next generation robotic systems," in *2022 30th Mediterranean conference on control and automation (MED)*. IEEE, 2022, pp. 487–493.
- [15] V. N. Sankaranarayanan, A. Saradagi, S. Satpute, and G. Nikolakopoulos, "A cbf-adaptive control architecture for visual navigation for uav in the presence of uncertainties," in *2024 IEEE International Conference on Robotics and Automation (ICRA)*, 2024, pp. 13 659–13 665.
- [16] A. S. Seisa, S. G. Satpute, B. Lindqvist, and G. Nikolakopoulos, "An edge-based architecture for offloading model predictive control for uavs," *Robotics*, vol. 11, no. 4, 2022. [Online]. Available: <https://www.mdpi.com/2218-6581/11/4/80>
- [17] S. Wilson, P. Glotfelter, L. Wang, S. Mayya, G. Notomista, M. Mote, and M. Egerstedt, "The robotarium: Globally impactful opportunities, challenges, and lessons learned in remote-access, distributed control of multirobot systems," *IEEE Control Systems Magazine*, vol. 40, no. 1, pp. 26–44, 2020.
- [18] R. Olfati-Saber, "Near-identity diffeomorphisms and exponential/spl epsi/-tracking and/spl epsi/-stabilization of first-order nonholonomic se (2) vehicles," in *Proceedings of the 2002 american control conference (iecc cat. no. ch37301)*, vol. 6. IEEE, 2002, pp. 4690–4695.